Composite Structures 94 (2012) 2118–2128

Contents lists available at SciVerse ScienceDirect

Composite Structures

journal homepage: www.elsevier.com/locate/compstruct

Ritz analysis of vibrating rectangular and skew multilayered plates based on advanced variable-kinematic models

Lorenzo Dozio [a,*], Erasmo Carrera [b]

[a] Department of Aerospace Engineering, Politecnico di Milano, via La Masa, 34, 20156 Milano, Italy
[b] Department of Mechanical and Aerospace Engineering, Politecnico di Torino, Corso Duca degli Abruzzi, 24, 10129 Torino, Italy

ARTICLE INFO

Article history:
Available online 14 February 2012

Keywords:
Free vibration
Multilayered plates
Variable-kinematic Ritz method
Layerwise plate theories

ABSTRACT

A variable-kinematic Ritz formulation based on two-dimensional higher-order layerwise and equivalent single-layer theories is described in this paper to accurately predict free vibration of thick and thin, rectangular and skew multilayered plates with clamped, free and simply-supported boundary conditions. The main result is the derivation at a layer level of so-called *Ritz fundamental nuclei* for the stiffness and mass matrices which are invariant with respect to both the assumed kinematic model and the type of Ritz functions. In this work, products of Chebyshev polynomials and boundary-compliant functions are chosen as admissible trial set. After studying the convergence of the method, its accuracy is evaluated, in terms of frequency parameters and through-the-thickness distribution of modal displacements, by comparison with some reference results available in the literature. Results for sandwich plates with soft core are given for the first time, which may serve as benchmark values for future research.

1. Introduction

With growing use of laminated composite and sandwich plates as primary structural components in many engineering applications, accurate assessment of their response is becoming more and more crucial. Contrary to single-layer metallic structures made of isotropic materials, multilayered constructions are typically characterized by high shear deformation. Displacements in the thickness direction may exhibit discontinuous derivatives in correspondence to each layer interface (the so-called *zig-zag* behavior). In addition, for equilibrium reasons, transverse shear and normal stresses should satisfy appropriate interlaminar continuity conditions.

Such complicating effects put great difficulties in achieving reliable prediction of the laminate mechanical behavior with traditional two-dimensional (2-D) models such as the classical plate theory (CPT) [1] or first-order shear deformation theory (FSDT) [2]. CPT and FSDT were originally proposed as axiomatic models for isotropic structures and then adapted to layered plates as equivalent single-layer (ESL) models with appropriate laminate stiffness properties [3]. Both theories rely on overly simplified assumptions concerning the three-dimensional (3-D) kinematics of deformation of the plate in accordance to the need of working with reasonable yet economical models that could be handled by hand or by the calculation capabilities available at the time they were derived.

Nowadays, computing capabilities allow overcoming the limitations of CPT and FSDT by using more refined theories encompassing an enriched set of kinematic variables, while preserving the 2-D nature of the models. In this way, more complicated problems, including static and dynamic response of laminated and sandwich plates with moderate thickness-to-length ratios or high degree of orthotropy, can be solved with better accuracy, without resorting to fully 3-D cumbersome analysis.

In the last three decades, much research has been made on advanced 2-D models of multilayered plates. The most common attempts involve displacement-based higher-order ESL theories, where the conventional single-layer displacement form of FSDT is enriched with various high-order terms as power series expansion of the thickness coordinate, and layerwise (LW) or discrete-layer formulations, in which two-dimensional approximations of the kinematic field are introduced at a layer level [4]. Investigations have been and are still currently focused on identifying which aspects of the 3-D plate behavior should be accounted for and properly modeled, with the aim of obtaining reliable formulations without unnecessary complexity. It is beyond the scope of the present study to review the extensive literature on laminated plate theories. Interested readers may refer, for example, to early survey papers [5,6] and to more recent review articles [7–10].

In contrast to classical plate models, the use of higher-order or layerwise theories typically lead to complex formulas and equations describing the structural problem. Derivation and computer implementation of advanced formulations would be less cumbersome with the availability of appropriate techniques capable of handling in an efficient and unified way arbitrary refinements of

* Corresponding author. Tel.: +39 02 2399 8329; fax: +39 02 2399 8334.
E-mail addresses: lorenzo.dozio@polimi.it (L. Dozio), erasmo.carrera@polito.it (E. Carrera).

0263-8223/$ - see front matter © 2012 Elsevier Ltd. All rights reserved.
doi:10.1016/j.compstruct.2012.02.008

traditional lamination theories. To this aim, a powerful approach was developed by Carrera [11] in the mid-nineties of the last century. It is a formal technique permitting to handle in an unified manner an infinite number of 2-D ESL and LW axiomatic plate and shell theories with *variable-kinematic* properties. The attribute *variable-kinematic* stands for the property of the formulation of being invariant with respect to the specific plate theory. In other words, the kinematics of the plate model, from the very simple to the very complex, can be conveniently changed without the need of a new mathematical development each time. Carrera's formulation was successfully implemented to obtain new Navier-type analytical solutions, finite element and meshless results using many different plate theories for bending, buckling and vibration problems of transversely anisotropic structures [12–17].

More recently, the same technique was employed to derive a variable-kinematic Ritz (*vk*-Ritz) method for vibration study of quadrilateral thin and thick plates [18]. Differently from Navier's solution method, the Ritz method is capable of providing upper-bound vibration solutions for plates with arbitrary laminate layups and boundary conditions. In addition, relying on a global approximation, the method has a high spectral accuracy and converge faster than local methods such as finite elements. As such, it can be quite suitable to provide benchmark reference values or during preliminary design studies and parametric analysis.

The *vk*-Ritz formulation presented in [18] was limited to free vibration of isotropic plates, thus only ESL refined theories were considered. Attention is focused in this study on extending the method to layerwise theories with the aim of providing a better description of the dynamic behavior of multilayered plates. In particular, rectangular and skew laminated composite and sandwich plates with different combination of simply-supported, free and clamped edges are considered. It has to be noted that a similar Ritz-based approach has been employed in [19]. However, the method was limited to rectangular anisotropic plates having simply-supported boundary conditions.

The present mathematical derivation is carried out at a layer level so that so-called *layer Ritz fundamental nuclei* of the mass and stiffness matrices are obtained. Details are given on the expansion of the layer nuclei and the assemblage from layer to multilayer level to obtain the mass and stiffness matrices of the whole plate. As shown in the following, higher-order ESL theories are recovered by simply using a summation over the layers of the plate as an assembly procedure. Fundamental nuclei of the *vk*-Ritz method are invariant also with respect to the type of Ritz trial set. Differently from [18], the kinematically admissible functions are taken here as the product of Chebyshev polynomials and boundary characteristic functions. It will be shown that this choice guarantees rapid convergence, numerical robustness and high accuracy.

2. The layerwise *vk*-Ritz formulation

A skew flat laminated plate of total thickness h and arbitrary boundary conditions is considered. The plate has side lengths a, b, and skew angle γ with respect to y axis as shown in Fig. 1. The plate consists of N_l layers, which are assumed to be homogeneous and made of orthotropic material. The kth layer has thickness h_k and is located between interfaces $z = z_k$ and $z = z_{k+1}$ in the thickness direction. In this work, the layer numbering begins at the bottom surface of the laminate (i.e., $z_1 = -h/2$). A four-letter compact symbolic notation is used for describing simply supported (S), clamped (C) and free (F) boundary conditions, numbered in a counterclockwise direction beginning from edge DA (see Fig. 1).

For generality and convenience, the present formulation is expressed in dimensionless coordinates using the following relationships:

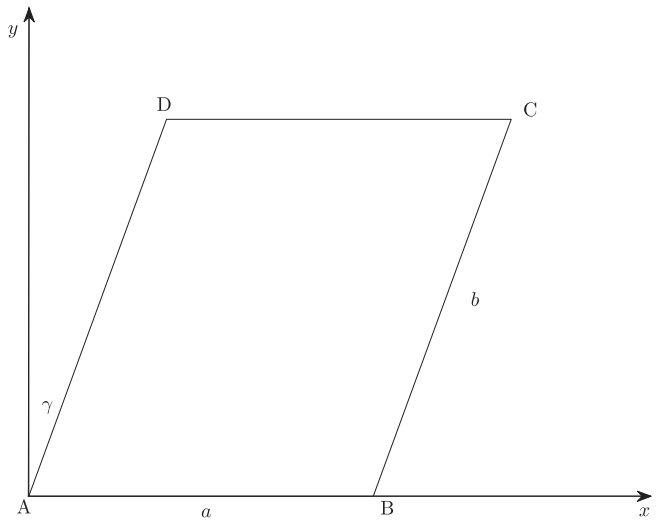

Fig. 1. Plate geometry.

$$\xi = \frac{2}{a}(x - y\tan\gamma) - 1 \tag{1}$$

$$\eta = \frac{2}{b}(y\sec\gamma) - 1 \tag{2}$$

$$\zeta_k = \frac{2}{h_k}z - \frac{z_{k+1} + z_k}{h_k} \tag{3}$$

where ζ_k is the local dimensionless layer coordinate ($-1 \leqslant \zeta_k \leqslant 1$). The derivatives of any quantity in the two coordinate systems are related by

$$\begin{Bmatrix} \frac{\partial}{\partial x} \\ \frac{\partial}{\partial y} \\ \frac{\partial}{\partial z} \end{Bmatrix} = \begin{bmatrix} \frac{2}{a} & 0 & 0 \\ -\frac{2}{a}\tan\gamma & \frac{2}{b}\sec\gamma & 0 \\ 0 & 0 & \frac{2}{h_k} \end{bmatrix} \begin{Bmatrix} \frac{\partial}{\partial \xi} \\ \frac{\partial}{\partial \eta} \\ \frac{\partial}{\partial \zeta_k} \end{Bmatrix} \tag{4}$$

The constitutive equation of a generic layer k can be written in the laminate reference coordinate system as follows:

$$\begin{aligned} \boldsymbol{\sigma}_p^k &= \widetilde{\mathbf{C}}_{pp}^k \boldsymbol{\epsilon}_p^k + \widetilde{\mathbf{C}}_{pn}^k \boldsymbol{\epsilon}_n^k \\ \boldsymbol{\sigma}_n^k &= \widetilde{\mathbf{C}}_{np}^k \boldsymbol{\epsilon}_p^k + \widetilde{\mathbf{C}}_{nn}^k \boldsymbol{\epsilon}_n^k \end{aligned} \tag{5}$$

where the stress vector $\boldsymbol{\sigma}^k$ and the strain vector $\boldsymbol{\epsilon}^k$ are split into in-plane and out-of-plane (normal) components, respectively,

$$\boldsymbol{\sigma}_p^k = \begin{Bmatrix} \sigma_{xx}^k \\ \sigma_{yy}^k \\ \sigma_{xy}^k \end{Bmatrix}, \quad \boldsymbol{\sigma}_n^k = \begin{Bmatrix} \sigma_{xz}^k \\ \sigma_{yz}^k \\ \sigma_{zz}^k \end{Bmatrix}, \quad \boldsymbol{\epsilon}_p^k = \begin{Bmatrix} \epsilon_{xx}^k \\ \epsilon_{yy}^k \\ \gamma_{xy}^k \end{Bmatrix}, \quad \boldsymbol{\epsilon}_n^k = \begin{Bmatrix} \gamma_{xz}^k \\ \gamma_{yz}^k \\ \epsilon_{zz}^k \end{Bmatrix} \tag{6}$$

The matrix of stiffness coefficients, $\widetilde{\mathbf{C}}^k$, follows a similar partition:

$$\begin{aligned} \widetilde{\mathbf{C}}_{pp}^k &= \begin{bmatrix} \widetilde{C}_{11}^k & \widetilde{C}_{12}^k & \widetilde{C}_{16}^k \\ \widetilde{C}_{12}^k & \widetilde{C}_{22}^k & \widetilde{C}_{26}^k \\ \widetilde{C}_{16}^k & \widetilde{C}_{26}^k & \widetilde{C}_{66}^k \end{bmatrix}, \quad \widetilde{\mathbf{C}}_{pn}^k = \begin{bmatrix} 0 & 0 & \widetilde{C}_{13}^k \\ 0 & 0 & \widetilde{C}_{23}^k \\ 0 & 0 & \widetilde{C}_{36}^k \end{bmatrix} \\ \widetilde{\mathbf{C}}_{np}^k &= \begin{bmatrix} 0 & 0 & 0 \\ 0 & 0 & 0 \\ \widetilde{C}_{13}^k & \widetilde{C}_{23}^k & \widetilde{C}_{36}^k \end{bmatrix}, \quad \widetilde{\mathbf{C}}_{nn}^k = \begin{bmatrix} \widetilde{C}_{55}^k & \widetilde{C}_{45}^k & 0 \\ \widetilde{C}_{45}^k & \widetilde{C}_{44}^k & 0 \\ 0 & 0 & \widetilde{C}_{33}^k \end{bmatrix} \end{aligned} \tag{7}$$

The stiffness constants $\widetilde{C}_{ij}^k$ are derived from the stiffness coefficients C_{ij}^k expressed in the layer reference system through a proper coordinate transformation [20].

According to the formulation proposed by Carrera in [11] and assuming harmonic motion with circular frequency ω, the dis-

placement vector for each k-th lamina $\mathbf{u}^k$ is expressed through an indicial notation over τ as follows:

$$\mathbf{u}^k(\xi,\eta,\zeta_k,t)=\begin{Bmatrix} u^k(\xi,\eta,\zeta_k,t)\\ v^k(\xi,\eta,\zeta_k,t)\\ w^k(\xi,\eta,\zeta_k,t)\end{Bmatrix}=\begin{Bmatrix} F_\tau(\zeta_k)\hat{u}^k_\tau(\xi,\eta)\\ F_\tau(\zeta_k)\hat{v}^k_\tau(\xi,\eta)\\ F_\tau(\zeta_k)\hat{w}^k_\tau(\xi,\eta)\end{Bmatrix}e^{j\omega t}=F_\tau(\zeta_k)\hat{\mathbf{u}}^k_\tau(\xi,\eta)e^{j\omega t} \tag{8}$$

in which $\tau = t, b, r$ $(r = 2,\ldots,N)$ is a theory-related index, where t stands for top surface and b stands for bottom surface, $F_\tau(\zeta_k)$ are assumed thickness functions, and $N \geqslant 1$ is the order of the theory. Note that in Eq. (8) the summation convention for repeated indices is implied, i.e.,

$$\mathbf{u}^k=\left(F_t\hat{\mathbf{u}}^k_t+F_2\hat{\mathbf{u}}^k_2+\cdots+F_N\hat{\mathbf{u}}^k_N+F_b\hat{\mathbf{u}}^k_b\right)e^{j\omega t} \tag{9}$$

Thickness functions $F_\tau(\zeta_k)$ can be arbitrarily selected to properly describe the assumed deformation profile of the plate in each layer (see Fig. 2). However, an effective way to satisfy the interlaminar continuity of the displacements is to choose

$$\begin{aligned} F_t(\zeta_k)&=\frac{1+\zeta_k}{2};\quad F_b(\zeta_k)=\frac{1-\zeta_k}{2};\quad F_r(\zeta_k)\\ &=P_r(\zeta_k)-P_{r-2}(\zeta_k)\quad r=2,3,\ldots,N\end{aligned} \tag{10}$$

where $P_i(\zeta_k)$ is the Legendre polynomial of ith order. In so doing, the displacement variables $\mathbf{u}^k_b$ and $\mathbf{u}^k_t$ are the actual values at the bottom and top surfaces of layer k, respectively, and the interlaminar continuity can be easily imposed as follows:

$$\hat{\mathbf{u}}^k_t=\hat{\mathbf{u}}^{k+1}_b\quad k=1,2,\ldots,N_l-1 \tag{11}$$

The formulation of Eq. (8) in conjunction with the set defined by Eq. (10) leads to an entire family of layerwise plate theories parametrized by the order N. They will be shortly indicated here by LDN. For example, LD2 theory is based on the following assumed displacement field for each layer k,

$$\begin{aligned} u^k&=\tfrac{1+\zeta_k}{2}\hat{u}^k_t+\tfrac{1-\zeta_k}{2}\hat{u}^k_b+\tfrac{3\zeta_k^2-3}{2}\hat{u}^k_2\\ v^k&=\tfrac{1+\zeta_k}{2}\hat{v}^k_t+\tfrac{1-\zeta_k}{2}\hat{v}^k_b+\tfrac{3\zeta_k^2-3}{2}\hat{v}^k_2\\ w^k&=\tfrac{1+\zeta_k}{2}\hat{w}^k_t+\tfrac{1-\zeta_k}{2}\hat{w}^k_b+\tfrac{3\zeta_k^2-3}{2}\hat{w}^k_2\end{aligned} \tag{12}$$

The number of displacement degrees of freedom for a given LDN theory depends upon the number of constitutive layers and is given by $3(N+1)N_l-3(N_l-1)$.

According to the outlined framework, the in-plane and out-of-plane strain components can be written in the following form

$$\boldsymbol{\epsilon}^k_p=F_\tau(\zeta_k)\mathbf{D}_p\hat{\mathbf{u}}^k_\tau(\xi,\eta)e^{j\omega t} \tag{13}$$

$$\boldsymbol{\epsilon}^k_n=F_\tau(\zeta_k)\mathbf{D}_n\hat{\mathbf{u}}^k_\tau(\xi,\eta)e^{j\omega t}+\frac{2}{h_k}\frac{dF_\tau}{d\zeta_k}(\zeta_k)\hat{\mathbf{u}}^k_\tau(\xi,\eta)e^{j\omega t} \tag{14}$$

where

$$\mathbf{D}_p=\begin{bmatrix} \frac{2}{a}\frac{\partial}{\partial\xi} & 0 & 0\\ 0 & \frac{2}{b}\sec\gamma\frac{\partial}{\partial\eta}-\frac{2}{a}\tan\gamma\frac{\partial}{\partial\xi} & 0\\ \frac{2}{b}\sec\gamma\frac{\partial}{\partial\eta}-\frac{2}{a}\tan\gamma\frac{\partial}{\partial\xi} & \frac{2}{a}\frac{\partial}{\partial\xi} & 0\end{bmatrix} \tag{15}$$

and

$$\mathbf{D}_n=\begin{bmatrix} 0 & 0 & \frac{2}{a}\frac{\partial}{\partial\xi}\\ 0 & 0 & \frac{2}{b}\sec\gamma\frac{\partial}{\partial\eta}-\frac{2}{a}\tan\gamma\frac{\partial}{\partial\xi}\\ 0 & 0 & 0\end{bmatrix} \tag{16}$$

Using Eqs. 5, 8, 13 and 14, the maximum potential energy $U_{\max}$ and the maximum kinetic energy $T_{\max}$ of the plate vibrating harmonically are given, respectively, by

$$\begin{aligned} U_{\max}=\frac{1}{2}\sum_{k=1}^{N_l}\int_{-1}^{+1}\int_{-1}^{+1}\Big[&\left(\mathbf{D}_p\hat{\mathbf{u}}^k_\tau\right)^{\mathrm{T}}\left(E^k_{\tau s}\mathbf{C}^k_{pp}\mathbf{D}_p\hat{\mathbf{u}}^k_s+E^k_{\tau s}\mathbf{C}^k_{pn}\mathbf{D}_n\hat{\mathbf{u}}^k_s+E^k_{\tau\partial s}\mathbf{C}^k_{pn}\hat{\mathbf{u}}^k_s\right)\\ &+\left(\mathbf{D}_n\hat{\mathbf{u}}^k_\tau\right)^{\mathrm{T}}\left(E^k_{\tau s}\mathbf{C}^k_{np}\mathbf{D}_p\hat{\mathbf{u}}^k_s+E^k_{\tau s}\mathbf{C}^k_{nn}\mathbf{D}_n\hat{\mathbf{u}}^k_s+E^k_{\tau\partial s}\mathbf{C}^k_{nn}\hat{\mathbf{u}}^k_s\right)\\ &+\hat{\mathbf{u}}^{k^{\mathrm{T}}}_\tau\left(E^k_{\partial\tau s}\mathbf{C}^k_{np}\mathbf{D}_p\hat{\mathbf{u}}^k_s+E^k_{\partial\tau s}\mathbf{C}^k_{nn}\mathbf{D}_n\hat{\mathbf{u}}^k_s+E^k_{\partial\tau\partial s}\mathbf{C}^k_{nn}\hat{\mathbf{u}}^k_s\right)\Big]\frac{ab}{4}\cos\gamma\,d\xi\,d\eta\end{aligned} \tag{17}$$

and

$$T_{\max}=\frac{1}{2}\omega^2\sum_{k=1}^{N_l}\int_{-1}^{+1}\int_{-1}^{+1}E^k_{\tau s}\rho^k\hat{\mathbf{u}}^{k^{\mathrm{T}}}_\tau\hat{\mathbf{u}}^k_s\frac{ab}{4}\cos\gamma\,d\xi\,d\eta \tag{18}$$

where ρ^k is the mass density of layer k and the following thickness integrals have been introduced:

$$\begin{aligned} E^k_{\tau s}&=\frac{h_k}{2}\int_{-1}^{+1}F_\tau F_s\,d\zeta_k\\ E^k_{\tau\partial s}&=\int_{-1}^{+1}F_\tau\frac{dF_s}{d\zeta_k}d\zeta_k\\ E^k_{\partial\tau s}&=\int_{-1}^{+1}\frac{dF_\tau}{d\zeta_k}F_s\,d\zeta_k\\ E^k_{\partial\tau\partial s}&=\frac{2}{h_k}\int_{-1}^{+1}\frac{dF_\tau}{d\zeta_k}\frac{dF_s}{d\zeta_k}d\zeta_k\end{aligned} \tag{19}$$

A standard Ritz solution is sought by expressing the components of each displacement unknown $\hat{\mathbf{u}}^k_\tau(\xi,\eta)$ as sets of two-dimensional finite series:

$$\begin{aligned} \hat{u}^k_\tau(\xi,\eta)&=\mathscr{N}_{u\tau i}(\xi,\eta)c^k_{u\tau i}\\ \hat{v}^k_\tau(\xi,\eta)&=\mathscr{N}_{v\tau i}(\xi,\eta)c^k_{v\tau i}\\ \hat{w}^k_\tau(\xi,\eta)&=\mathscr{N}_{w\tau i}(\xi,\eta)c^k_{w\tau i}\\ (i&=1,2,\ldots,M)\end{aligned} \tag{20}$$

where M is the order of the Ritz expansion, $c^k_{u\tau i}$, $c^k_{v\tau i}$ and $c^k_{w\tau i}$ are unknown coefficients, $\mathscr{N}_{u\tau i}$, $\mathscr{N}_{v\tau i}$ and $\mathscr{N}_{w\tau i}$ are the corresponding assumed shape functions, and i is the Ritz-related index. Note that the summation convention over the repeated Ritz-related index i is

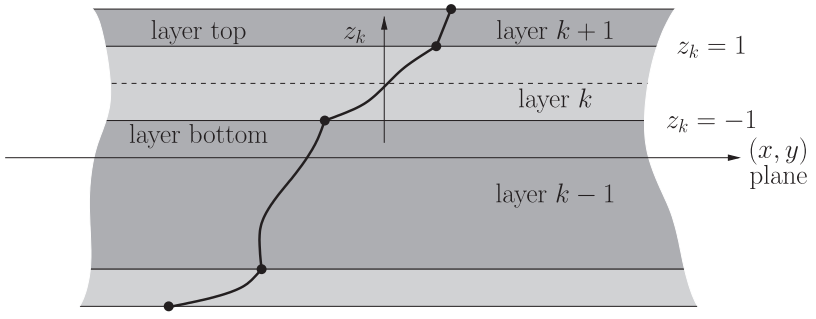

Fig. 2. Example of through-the-thickness displacement in case of layerwise theories.

implied. In this work, boundary conditions are considered to be homogeneous through the height of the same edge section, i.e., identical conditions are imposed in each layer of the plate edge. This is the reason the in-plane Ritz functions $\mathscr{N}_{\delta\tau i}$ $(\delta = u, v, w)$ are layer-independent. Convergence to the exact solution is guaranteed as $M \to \infty$ if the trial functions are admissible functions, i.e., they are a complete set of geometrically-compliant functions which are required to satisfy only the essential (displacement) boundary conditions. The i-th admissible function is chosen here as

$$\mathscr{N}_{\delta\tau i}(\xi,\eta) = \phi_{\delta\tau m}(\xi)\psi_{\delta\tau n}(\eta) \quad (m,n = 1,2,\ldots,P) \tag{21}$$

where

$$\phi_{\delta\tau m}(\xi) = f_{\delta\tau}(\xi)p_m(\xi) \tag{22}$$

$$\psi_{\delta\tau n}(\eta) = g_{\delta\tau}(\eta)p_n(\eta) \tag{23}$$

P is the order of expansion in each direction ξ and η, and

$$p_l(\chi) = \cos\left[(l-1)\arccos(\chi)\right] \quad (l = m,n;\chi = \xi,\eta) \tag{24}$$

is the one-dimensional Chebyshev polynomial along χ direction. The Chebyshev polynomial set is a complete and orthogonal series in the interval $[-1,+1]$. This ensures that better convergence and numerical stability can be accomplished compared with other polynomial set [21]. $f(\xi)$ and $g(\eta)$ are boundary functions corresponding to the type of boundary conditions along ξ and η, respectively, and are reported in Table 1. The order M of the Ritz expansion is given by $M = P^2$ and the indices i, m, and n are related by the expression $i = P(m-1)+n$.

For the sake of compact notation, Eq. (20) is rearranged in matrix form as follows

$$\hat{\mathbf{u}}^k_\tau(\xi,\eta) = \boldsymbol{N}_{\tau i}(\xi,\eta)\mathbf{c}^k_{\tau i} \tag{25}$$

in which

$$\boldsymbol{N}_{\tau i}(\xi,\eta) = \mathrm{diag}(\mathscr{N}_{u\tau i}, \mathscr{N}_{v\tau i}, \mathscr{N}_{w\tau i}) \tag{26}$$

$$\mathbf{c}^k_{\tau i} = \left[c^k_{u\tau i}\ c^k_{v\tau i}\ c^k_{w\tau i}\right]^{\mathrm{T}} \tag{27}$$

Substituting Eq. (25) into Eqs. (17) and (18), one obtains the potential and kinetic energy of the plate, respectively, as a summation of layer contributions as follows:

$$U_{\max} = \frac{1}{2}\sum_{k=1}^{N_l}\mathbf{c}^{k\mathrm{T}}_{\tau i}\mathbf{K}^k_{\tau s ij}\mathbf{c}^k_{sj} \tag{28}$$

$$T_{\max} = \frac{1}{2}\omega^2\sum_{k=1}^{N_l}\mathbf{c}^{k\mathrm{T}}_{\tau i}\mathbf{M}^k_{\tau s ij}\mathbf{c}^k_{sj} \tag{29}$$

where

$$\begin{aligned}\mathbf{K}^k_{\tau s ij} = \int_{-1}^{+1}\int_{-1}^{+1}\Big[&(\mathbf{D}_p\boldsymbol{N}_{\tau i})^{\mathrm{T}}\left(E^k_{\tau s}\mathbf{C}^k_{pp}\mathbf{D}_p\boldsymbol{N}_{sj} + E^k_{\tau s}\mathbf{C}^k_{pn}\mathbf{D}_n\boldsymbol{N}_{sj} + E^k_{\tau\partial s}\mathbf{C}^k_{pn}\boldsymbol{N}_{sj}\right)\\ &+(\mathbf{D}_n\boldsymbol{N}_{\tau i})^{\mathrm{T}}\left(E^k_{\tau s}\mathbf{C}^k_{np}\mathbf{D}_p\boldsymbol{N}_{sj} + E^k_{\tau s}\mathbf{C}^k_{nn}\mathbf{D}_n\boldsymbol{N}_{sj} + E^k_{\tau\partial s}\mathbf{C}^k_{nn}\boldsymbol{N}_{sj}\right)\\ &+\boldsymbol{N}^{\mathrm{T}}_{\tau i}\left(E^k_{\partial\tau s}\mathbf{C}^k_{np}\mathbf{D}_p\boldsymbol{N}_{sj} + E^k_{\partial\tau s}\mathbf{C}^k_{nn}\mathbf{D}_n\boldsymbol{N}_{sj} + E^k_{\partial\tau\partial s}\mathbf{C}^k_{nn}\boldsymbol{N}_{sj}\right)\Big]\frac{ab}{4}\cos\gamma\, d\xi d\eta\end{aligned} \tag{30}$$

Table 1
Boundary functions.

Boundary condition	$f_{u\tau}$	$f_{v\tau}$	$f_{w\tau}$	$g_{u\tau}$	$g_{v\tau}$	$g_{w\tau}$
C–C	$1-\xi^2$	$1-\xi^2$	$1-\xi^2$	$1-\eta^2$	$1-\eta^2$	$1-\eta^2$
S–S	1	$1-\xi^2$	$1-\xi^2$	$1-\eta^2$	1	$1-\eta^2$
F–F	1	1	1	1	1	1
C–S	$1+\xi$	$1-\xi^2$	$1-\xi^2$	$1-\eta^2$	$1+\eta$	$1-\eta^2$
S–C	$1-\xi$	$1-\xi^2$	$1-\xi^2$	$1-\eta^2$	$1-\eta$	$1-\eta^2$
C–F	$1+\xi$	$1+\xi$	$1+\xi$	$1+\eta$	$1+\eta$	$1+\eta$
F–C	$1-\xi$	$1-\xi$	$1-\xi$	$1-\eta$	$1-\eta$	$1-\eta$
S–F	1	$1+\xi$	$1+\xi$	$1+\eta$	1	$1+\eta$
F–S	1	$1-\xi$	$1-\xi$	$1-\eta$	1	$1-\eta$

$$\mathbf{M}^k_{\tau s ij} = \int_{-1}^{+1}\int_{-1}^{+1}E^k_{\tau s}\rho^k\boldsymbol{N}^{\mathrm{T}}_{\tau i}\boldsymbol{N}_{sj}\frac{ab}{4}\cos\gamma\, d\xi d\eta \tag{31}$$

are 3×3 matrices representing the *layer Ritz fundamental nuclei* of the formulation. The nine terms of the Ritz nuclei are given explicitly in the Appendix.

The plate stiffness and mass matrices can be built from the above derived nuclei by an assembly-like procedure. First, the fundamental nuclei are expanded at a layer level through variation of the theory-related indices τ and s over the previously defined ranges. For example, the following $3(N+1)\times 3(N+1)$ layer-level stiffness matrix is obtained:

$$\mathbf{K}^k_{ij} = \begin{bmatrix}\mathbf{K}^k_{ttij} & \mathbf{K}^k_{trij} & \mathbf{K}^k_{tbij}\\ \mathbf{K}^k_{rtij} & \mathbf{K}^k_{rrij} & \mathbf{K}^k_{rbij}\\ \mathbf{K}^k_{btij} & \mathbf{K}^k_{brij} & \mathbf{K}^k_{bbij}\end{bmatrix} \tag{32}$$

where $r = 2, \ldots, N$. According to the assumed discrete-layer kinematics, resulting matrices are then assembled from layer to multilayer level by enforcing the interlaminar continuity condition Eq. (11). This yields

$$\mathbf{K}^{\mathrm{LW}}_{ij} = \begin{bmatrix}\ddots & & & & & & \\ & \mathbf{K}^{k+1}_{ttij} & \mathbf{K}^{k+1}_{trij} & \mathbf{K}^{k+1}_{tbij} & & & \\ & \mathbf{K}^{k+1}_{rtij} & \mathbf{K}^{k+1}_{rrij} & \mathbf{K}^{k+1}_{rbij} & & & \\ & \mathbf{K}^{k+1}_{btij} & \mathbf{K}^{k+1}_{brij} & \mathbf{K}^{k+1}_{bbij}+\mathbf{K}^k_{ttij} & \mathbf{K}^k_{trij} & \mathbf{K}^k_{tbij} & \\ & & & \mathbf{K}^k_{rtij} & \mathbf{K}^k_{rrij} & \mathbf{K}^k_{rbij} & \\ & & & \mathbf{K}^k_{btij} & \mathbf{K}^k_{brij} & \mathbf{K}^k_{bbij}+\mathbf{K}^{k-1}_{ttij} & \\ & & & & & & \ddots\end{bmatrix} \tag{33}$$

for the layerwise-based stiffness matrix, and an identical structure for the layerwise-based mass matrix $\mathbf{M}^{\mathrm{LW}}_{ij}$. Finally, the plate stiffness and mass matrices $\mathbf{K}^{\mathrm{LW}}$ and $\mathbf{M}^{\mathrm{LW}}$ are obtained by expanding the multilayer matrices $\mathbf{K}^{\mathrm{LW}}_{ij}$ and $\mathbf{M}^{\mathrm{LW}}_{ij}$ through variation of Ritz-related indices i and j, following a similar to nuclei-to-layer expansion, as

$$\mathbf{K}^{\mathrm{LW}} = \begin{bmatrix}\mathbf{K}^{\mathrm{LW}}_{11} & \mathbf{K}^{\mathrm{LW}}_{12} & \ldots & \mathbf{K}^{\mathrm{LW}}_{1M}\\ \mathbf{K}^{\mathrm{LW}}_{21} & \mathbf{K}^{\mathrm{LW}}_{22} & \ldots & \mathbf{K}^{\mathrm{LW}}_{2M}\\ \vdots & & & \\ \mathbf{K}^{\mathrm{LW}}_{M1} & \mathbf{K}^{\mathrm{LW}}_{M2} & \ldots & \mathbf{K}^{\mathrm{LW}}_{MM}\end{bmatrix} \tag{34}$$

and

$$\mathbf{M}^{\mathrm{LW}} = \begin{bmatrix}\mathbf{M}^{\mathrm{LW}}_{11} & \mathbf{M}^{\mathrm{LW}}_{12} & \ldots & \mathbf{M}^{\mathrm{LW}}_{1M}\\ \mathbf{M}^{\mathrm{LW}}_{21} & \mathbf{M}^{\mathrm{LW}}_{22} & \ldots & \mathbf{M}^{\mathrm{LW}}_{2M}\\ \vdots & & & \\ \mathbf{M}^{\mathrm{LW}}_{M1} & \mathbf{M}^{\mathrm{LW}}_{M2} & \ldots & \mathbf{M}^{\mathrm{LW}}_{MM}\end{bmatrix} \tag{35}$$

Matrices $\mathbf{K}^{\mathrm{LW}}$ and $\mathbf{M}^{\mathrm{LW}}$ have dimensions $[3(N+1)N_l - 3(N_l-1)]M \times [3(N+1)N_l - 3(N_l-1)]M$ for a given LDN theory and a M-term Ritz expansion.

By minimization of the energy functional $\Pi = U_{\max} - T_{\max}$ with respect to the vector of coefficients $\mathbf{c}^k_{\tau i}$, we obtain the standard generalized eigenvalue problem:

$$\left[\mathbf{K}^{\mathrm{LW}} - \omega^2\mathbf{M}^{\mathrm{LW}}\right]\mathbf{c} = \mathbf{0} \tag{36}$$

where $\mathbf{c}$ is the vector collecting the unknown Ritz coefficients $\mathbf{c}^k_{sj}$.

3. Specialization for higher-order ESL theories

Eq. (8) can be also used to represent higher-order ESL theories. In this case, the superscript k is dropped and global thickness functions $F_\tau(z)$ are adopted, see Fig. 3. In this work, the z expansion is implemented via Taylor polynomials and related ESL theories will be shortly denoted by the acronym EDN, where N denotes the order of the expansion [18]. For example, ED3 is a third-order theory assuming the following displacement field:

$$\begin{aligned} u &= \hat{u}_0 + z\hat{u}_1 + z^2\hat{u}_2 + z^3\hat{u}_3 \\ v &= \hat{v}_0 + z\hat{v}_1 + z^2\hat{v}_2 + z^3\hat{v}_3 \\ w &= \hat{w}_0 + z\hat{w}_1 + z^2\hat{w}_2 + z^3\hat{w}_3 \end{aligned} \tag{37}$$

The total number of displacement variables of a EDN theory is $3(N+1)$. In the ESL case, since the displacement unknowns are the same for each layer, layer-level matrices are simply accumulated layer by layer,

$$\mathbf{K}_{ij}^{\mathrm{ESL}} = \sum_{k=1}^{N_l} \mathbf{K}_{ij}^k, \quad \mathbf{M}_{ij}^{\mathrm{ESL}} = \sum_{k=1}^{N_l} \mathbf{M}_{ij}^k \tag{38}$$

The final plate matrices $\mathbf{K}^{\mathrm{ESL}}$ and $\mathbf{M}^{\mathrm{ESL}}$, of dimensions $3M(N+1) \times 3M(N+1)$, are obtained by varying the Ritz-related indices i and j from 1 to M in the same way as the corresponding layerwise-based matrices.

Note that the first-order shear deformation theory (FSDT) can be easily recovered from ED1 theory after imposing the condition of null transverse normal stresses σ_{zz}^k and introducing a shear correction factor χ. The corresponding modified elastic coefficients are given by:

$$\begin{aligned} \widetilde{C}_{ij}^k &= C_{ij}^k - \frac{C_{i3}^k C_{j3}^k}{C_{33}^k} \quad (i,j = 1,2) \\ \widetilde{C}_{ii}^k &= \chi C_{ii}^k \quad (i = 4,5) \end{aligned} \tag{39}$$

4. Convergence of the method

The approximation obtained by the Ritz method can be made as accurate as desired by arbitrarily increasing the number of terms in the assumed series of Eq. (20). In practice, the number of Ritz terms is truncated to a finite value M due to computational time and capability. Therefore, the accuracy of the approximate solution resulting from the M-dimensional problem is affected by the rate of convergence associated with the choice of the set of trial functions. Convergence properties of the proposed method are here briefly discussed with respect to two representative cases.

The first case refers to a simply-supported (SSSS) square cross-ply [0°/90°] plate with thickness-to-length ratio $h/b = 0.1$. The two layers of equal thickness are made of an orthotropic material with the following non-dimensional properties: $E_1 = 25.1$, $E_2 = 4.8$, $E_3 = 0.75$, $G_{12} = 1.36$, $G_{13} = 1.2$, $G_{23} = 0.47$, $\nu_{12} = 0.036$, $\nu_{13} = 0.25$, $\nu_{23} = 0.171$, $\rho = 1$. Frequency parameters $\lambda = \omega h\sqrt{\rho/E_2}$ are shown in Table 2 corresponding to modes with wave numbers (1,1), (1,2) and (2,2). Illustrative results computed on the basis of ED2 and LD3 plate theories are reported for some increasing values of degree P. It can be observed that, as expected, convergence is monotonic from above as Ritz terms are added. Accurate (i.e., well-converged) frequencies to at least five significant figures are obtained when $P = 9$. Note that the trend is similar both for ED2 and LD3 models. Note also that Ritz solutions yield slightly different converged upper-bound values if ED2 or LD3 theory is used. As shown in the next section, the type of kinematic theory, if layer independent or dependent, and the corresponding order N can strongly affect accuracy of the solution.

The second case refers to a fully clamped (CCCC) skew laminated plate with aspect ratio $a/b = 1$, length-to-thickness ratio $a/h = 10$ and symmetric layup [90°/0°/90°/0°/90°]. Layers are of the same thickness and material with properties: $E_1/E_2 = 40$, $E_3 = E_2$, $G_{12} = G_{13} = 0.6E_2$, $G_{23} = 0.5E_2$, $\nu_{12} = \nu_{13} = \nu_{23} = 0.25$. Table 3 shows the first six non-dimensional frequencies $\lambda = (\omega b^2/\pi^2 h)\sqrt{\rho/E_2}$ for two skew angles $\gamma = 0°$ and 45°. For the sake of illustration, results computed using a second-order layerwise theory (LD2) are presented with degree P varying from 8 up to 13. Similarly to what found in the previous case, Ritz solutions converge monotonically from above to upper-bound values. However, one can notice that the rate of convergence is rather low for this case. In other words, the number P of terms required to obtain converged modal parameters to five digits is substantially higher than the above example. Note also that this fact is observed irrespective of the plate skew angle. It appears that the reason for such behavior is related to clamped boundary conditions, which are characterized by local displacement gradients near the edge difficult to be well approximated by global polynomials of relatively low order. Despite the slower convergence, reasonably accurate solutions can be attained with $P \leqslant 12$.

5. Illustrative examples

The *vk*-Ritz formulation derived thus far is validated in this section by comparison with some case studies available in the open

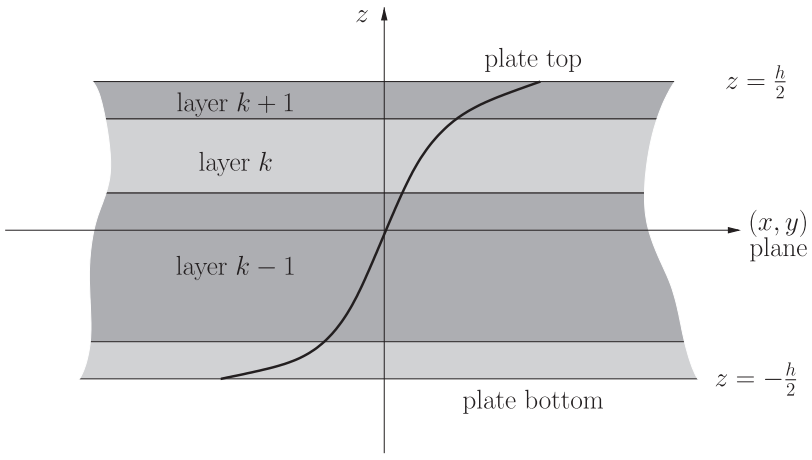

Fig. 3. Example of through-the-thickness displacement in case of equivalent-single-layer theories.

Table 2
Convergence study of a square simply-supported cross-ply [0°/90°] plate with $h/b = 0.1$. Material properties: $E_1 = 25.1$, $E_2 = 4.8$, $E_3 = 0.75$, $G_{12} = 1.36$, $G_{13} = 1.2$, $G_{23} = 0.47$, $\nu_{12} = 0.036$, $\nu_{13} = 0.25$, $\nu_{23} = 0.171$.

Theory	P	Mode		
		(1,1)	(1,2)	(2,2)
ED2	6	0.06333	0.14986	0.22477
	7	0.06093	0.14893	0.22304
	8	0.06093	0.14893	0.20835
	9	0.06093	0.14893	0.20810
	10	0.06093	0.14893	0.20810
	11	0.06093	0.14893	0.20810
	12	0.06093	0.14893	0.20810
LD3	6	0.06261	0.14628	0.21776
	7	0.06028	0.14539	0.21621
	8	0.06027	0.14539	0.20252
	9	0.06027	0.14539	0.20229
	10	0.06027	0.14539	0.20229
	11	0.06027	0.14539	0.20229
	12	0.06027	0.14539	0.20229

Table 3
Convergence study of a rhombic clamped cross-ply [90°/0°/90°/0°/90°] plate with $a/h = 10$. Material properties: $E_1/E_2 = 40$, $E_3 = E_2$, $G_{12} = G_{13} = 0.6E_2$, $G_{23} = 0.5E_2$, $\nu_{12} = \nu_{13} = \nu_{23} = 0.25$.

Skew angle (°)	P	Mode					
		1	2	3	4	5	6
0	8	2.3413	3.4795	4.1746	4.9248	5.0939	6.1898
	10	2.3409	3.4779	4.1742	4.9235	5.0897	6.1862
	11	2.3408	3.4776	4.1741	4.9233	5.0888	6.1854
	12	2.3408	3.4772	4.1740	4.9230	5.0884	6.1851
	13	2.3407	3.4771	4.1740	4.9229	5.0879	6.1847
45	8	3.4840	4.6504	5.7934	6.4653	6.9248	7.9081
	10	3.4834	4.6495	5.7917	6.4634	6.9159	7.8975
	11	3.4833	4.6492	5.7914	6.4631	6.9155	7.8970
	12	3.4832	4.6491	5.7913	6.4629	6.9154	7.8968
	13	3.4831	4.6490	5.7912	6.4628	6.9153	7.8966

literature. A brief discussion on results for natural frequencies obtained by the proposed method with those from three-dimensional and other two-dimensional approaches is presented. Both composite laminated and sandwich plates of rectangular and skew in-plane planform with various layups and boundary conditions are considered. New results on sandwich plates with laminated face sheets and a flexible isotropic core are also given in tabulated form, which may serve as benchmark values for future comparison.

5.1. Example 1: simply-supported square cross-ply plates

The fundamental frequency parameters $\lambda = (\omega b^2/h)\sqrt{\rho/E_2}$ of cross-ply unsymmetric [0°/90°] and four-layer symmetric [0°/90°/90°/0°] square laminated plates with all simply-supported edge conditions (SSSS) are presented in Table 4. The orthotropic material properties of individual layers are: $E_1/E_2 = 40$, $E_3 = E_2$, $G_{12} = G_{13} = 0.6E_2$, $G_{23} = 0.5E_2$ and $\nu_{12} = \nu_{13} = \nu_{23} = 0.25$. Each layer is assumed to be of equal thickness and mass density ρ. For the sake of comparison, three-dimensional elasticity solutions obtained by Chen and Lue [22] through a semi-analytical method combining the state space approach with the differential quadrature method are also given. Results are shown for various length-to-thickness ratios ($b/h = 5, 10, 20, 25, 50, 100$), thus encompassing both thin, moderately thick, and very thick plates, using kinematic theories of increasing complexity, from the simplest FSDT to high-order ESL theories and more refined LW models up to fourth order. The shear correction factor introduced in FSDT is arbitrarily taken to be $\chi = 5/6$. According to the outcomes of the convergence analysis, tabulated solutions are obtained with an order $P = 12$ of the Ritz expansion.

As expected, the degree of accuracy of the present 2-D results with respect to 3-D analysis improves by increasing the length-to-thickness ratio (from thick to thin plates) and the order of theory (for example, from LD1 to LD4). Excellent agreement is observed in all cases using a fourth-order layerwise theory, which appears to yield the exact frequency values independently from the plate parameters. However, it can be seen from Table 4 that a layerwise kinematic approximation of the mechanics of the plate may give worse predictions than a global through-the-thickness description. For example, in the unsymmetric [0°/90°] case, comparison of solutions computed by ED4 and LD2 theories, which leads in this example to models having the same number of degrees of freedom, shows that the ESL approach slightly outperforms the LW modeling in providing lower values of the fundamental frequency. As a final remark, it is worth pointing out that ESL models of moderate order are enough to get reasonably accurate results for the cases analyzed here.

5.2. Example 2: square laminated plates with various boundary conditions

Three different two-layer laminated square plates with distinct lamination schemes and boundary conditions involving combinations of clamped and free edges are analyzed in this example. The cases considered are: (1) a fully clamped (CCCC) plate with layup [−30°/45°]; (2) a plate with two opposite edges clamped and the others free (FCFC) having layup [0°/45°]; and (3) a cross-ply [0°/90°] plate with two adjacent edges clamped and two adjacent edges free (FCCF). All layers are assumed to be of the same thickness and density and made of the same material with the following properties: $E_1/E_2 = 25$, $E_3 = E_2$, $G_{12} = G_{13} = 0.5E_2$, $G_{23} = 0.2E_2$ and $\nu_{12} = \nu_{13} = \nu_{23} = 0.25$. The first four frequency parameters $\lambda = (\omega a^2/h)\sqrt{\rho/E_2}$ computed using the present formulation with two higher-order ESL theories (ED4 and ED6) and four layerwise theories LDN with N ranging from 1 to 4 are compared in Table 5 with finite element results available in [23]. For the sake of comparison, very thick plates with $a/h = 4$ are considered. Note that solutions of Ref. [23] are obtained either by the commercial code NASTRAN using standard 3-D brick elements either by an ad hoc formulation of 2-D layerwise plate elements based upon Reissner's mixed variation theorem. Also reported in Table 5 is number of degrees of freedom (dof) used in each model. Present results rely on Ritz expansion with $P = 10$.

It can be observed the close agreement for the first four modes between Ritz-based solutions and finite element analysis. It is confirmed that the Ritz approach is capable of yielding highly accurate results for arbitrary lamination layups and boundary conditions using models of reduced size. As before, despite the same number of degrees of freedom, ED4 models appears to be slightly more effective than LD2 models. However, this is not true if higher orders are adopted. Comparison between LD3 and LD4 theories shows that negligible improvement in accuracy is achieved beyond a certain model refinement. Note also that, from an engineering point of view, acceptable solutions for the cases considered in this example are obtained using models based on ESL theories.

5.3. Example 3: fully clamped skew laminated plates

The free vibration of fully clamped, four-layer, antisymmetric cross-ply [0°/90°/0°/90°] and angle-ply [45°/ − 45°/45°/ − 45°] rhombic laminates with thickness-to-length ratio $h/a = 0.1$ and two skew angles $\gamma = 30°, 45°$ are here analyzed. As before, the layers are of equal thickness and material. Material properties are those used in Example 1. Results in terms of the first eight fre-

Table 4
Fundamental frequency parameters $\lambda = \frac{\omega b^2}{h}\sqrt{\frac{\rho}{E_2}}$ of simply-supported square cross-ply laminated plates. Material properties: $E_1/E_2 = 40$, $E_3 = E_2$, $G_{12} = G_{13} = 0.6E_2$, $G_{23} = 0.5E_2$, $\nu_{12} = \nu_{13} = \nu_{23} = 0.25$.

Layup	Theory	b/h					
		5	10	20	25	50	100
[0°/90°]	3-D [22]	8.52690	10.3365	11.0368	11.1312	11.2636	11.2973
	FSDT	8.83331	10.4731	11.0779	11.1590	11.2705	11.2990
	ED2	8.79974	10.4638	11.0760	11.1579	11.2704	11.2992
	ED4	8.58316	10.3646	11.0456	11.1379	11.2652	11.2978
	LD1	8.73440	10.4531	11.0941	11.1803	11.2987	11.3290
	LD2	8.68860	10.4144	11.0609	11.1479	11.2677	11.2983
	LD3	8.52725	10.3364	11.0367	11.1320	11.2635	11.2972
	LD4	8.52704	10.3364	11.0367	11.1320	11.2635	11.2972
[0°/90°/90°/0°]	3-D [22]	10.6822	15.0687	17.6356	18.0548	18.6701	18.8353
	FSDT	10.8540	15.1426	17.6596	18.0708	18.6742	18.8362
	ED4	10.7608	15.1043	17.6470	18.0624	18.6720	18.8357
	LD1	10.8915	15.2192	17.6996	18.1003	18.6859	18.8427
	LD2	10.6914	15.0718	17.6364	18.0553	18.6701	18.8352
	LD3	10.6822	15.0686	17.6355	18.0547	18.6699	18.8351
	LD4	10.6821	15.0686	17.6355	18.0547	18.6699	18.8351

Table 5
First four frequency parameters $\lambda = \frac{\omega a^2}{h}\sqrt{\frac{\rho}{E_2}}$ of thick square composite plates ($a/h = 4$) with different lamination schemes and boundary conditions. Material properties: $E_1/E_2 = 25$, $E_3 = E_2$, $G_{12} = G_{13} = 0.5E_2$, $G_{23} = 0.2E_2$, $\nu_{12} = \nu_{13} = \nu_{23} = 0.25$.

Case	Mode	Theory						NASTRAN	Mixed LW
		ED4 (dof): (1500)	ED6 (2100)	LD1 (900)	LD2 (1500)	LD3 (2100)	LD4 (2700)	(3-D) [23] (26250)	FEM [23] (3267)
CCCC [−30°/45°]	1	8.859	8.772	9.103	8.954	8.740	8.736	8.859	8.760
	2	13.660	13.522	14.043	13.777	13.480	13.471	13.606	13.534
	3	14.837	14.667	15.191	14.979	14.630	14.620	14.786	14.684
	4	18.715	18.508	19.246	18.865	18.467	18.452	18.566	18.540
FCFC [0°/45°]	1	4.946	4.918	5.112	4.966	4.903	4.901	4.953	4.925
	2	5.956	5.928	6.150	5.989	5.913	5.911	5.953	5.937
	3	10.018	9.972	10.175	10.036	9.954	9.949	10.007	10.013
	4	10.591	10.555	10.814	10.611	10.541	10.537	10.583	10.592
FCCF [0°/90°]	1	2.804	2.794	2.845	2.821	2.788	2.787	2.804	2.790
	2	7.510	7.454	7.674	7.587	7.435	7.432	7.494	7.443
	3	7.748	7.689	7.928	7.827	7.667	7.664	7.735	7.675
	4	11.106	11.017	11.315	11.187	10.986	10.981	11.032	11.006

Table 6
First eight frequency parameters $\lambda = \frac{\omega b^2}{h\pi^2}\sqrt{\frac{\rho}{E_2}}$ of clamped antisymmetric cross-ply and angle-ply skew laminated plates with $h/a = 0.1$. Material properties: $E_1/E_2 = 40$, $E_3 = E_2$, $G_{12} = G_{13} = 0.6E_2$, $G_{23} = 0.5E_2$, $\nu_{12} = \nu_{13} = \nu_{23} = 0.25$.

Layup	Skew angle (°)	Theory	Mode							
			1	2	3	4	5	6	7	8
[0°/90°/0°/90°]	30	FSDT [25]	2.7796	4.1564	4.9237	5.3983	6.7204	6.7240	7.2729	8.0467
		HOST [24]	2.6666	3.9851	4.7227	5.1752	6.4445	6.4510	6.9755	7.7218
		LD1	2.6763	4.0044	4.7487	5.2033	6.4812	6.4888	7.0183	7.7656
		LD2	2.6209	3.9214	4.6512	5.0961	6.3493	6.3573	6.8774	7.6111
		LD3	2.6166	3.9125	4.6392	5.0824	6.3296	6.3374	6.8538	7.5846
	45	FSDT [25]	3.4430	4.8219	6.0850	6.2414	7.3720	8.0239	8.6233	9.3320
		HOST [24]	3.3015	4.6290	5.8423	6.0039	7.0792	7.7269	8.2726	8.9874
		LD1	3.3178	4.6559	5.8777	6.0437	7.1209	7.7781	8.3164	9.0444
		LD2	3.2482	4.5606	5.7587	5.9252	6.9787	7.6286	8.1531	8.8750
		LD3	3.2412	4.5484	5.7408	5.9058	6.9542	7.6010	8.1209	8.8378
[45°/−45°/45°/−45°]	30	FSDT [25]	2.7416	4.1219	4.9126	5.4395	6.6183	6.7842	7.2753	8.0427
		HOST [24]	2.6325	3.9549	4.7125	5.2107	6.3577	6.4954	6.9760	7.7176
		LD1	2.6422	3.9737	4.7378	5.2379	6.3954	6.5315	7.0178	7.7620
		LD2	2.5885	3.8917	4.6407	5.1283	6.2670	6.3954	6.8762	7.6077
		LD3	2.5843	3.8834	4.6289	5.1149	6.2488	6.3758	6.8529	7.5811
	45	FSDT [25]	3.4430	4.8219	6.0850	6.2414	7.3720	8.0239	8.6233	9.3320
		HOST [24]	3.3015	4.6290	5.8423	6.0039	7.0792	7.7269	8.2726	8.9874
		LD1	3.3178	4.6559	5.8777	6.0437	7.1209	7.7781	8.3164	9.0444
		LD2	3.2482	4.5606	5.7587	5.9252	6.9787	7.6286	8.1531	8.8750
		LD3	3.2412	4.5484	5.7408	5.9058	6.9542	7.6010	8.1209	8.8378

Table 7
Material properties of the face sheets and isotropic core for the sandwich plate in Example 4.

Component	Elastic modulus (GPa)	Poisson's ratio	Shear modulus (GPa)	Density (kg/m^3)
Face sheets	$E_1 = 131$ $E_2 = 10.34$ $E_3 = 10.34$	$\nu_{12} = 0.22$ $\nu_{13} = 0.22$ $\nu_{23} = 0.49$	$G_{12} = 6.895$ $G_{13} = 6.205$ $G_{23} = 6.895$	$\rho = 1627$
Core	$E_c = 6.89 \times 10^{-3}$	$\nu_c = 0$	$G_c = 3.45 \times 10^{-3}$	$\rho_c = 97$

Table 8
Frequency parameters $\lambda = \frac{\omega b^2}{h}\sqrt{\frac{\rho}{E_2}}$ of simply-supported plates with $a/b = 1$ and material properties listed in Table 7.

h/a	(m,n)	Theory						Ref. [26]
		FSDT	ED4	ED5	LD1	LD2	LD3	
0.01	(1,1)	16.2726	15.5454	12.8426	11.9463	11.9457	11.9457	11.9401
	(1,2)	44.8813	39.2593	26.3405	23.4160	23.4140	23.4140	23.4017
	(1,3)	95.3255	73.4859	41.6706	36.1694	36.1634	36.1634	36.1434
	(2,2)	64.7389	55.1383	35.1669	30.9640	30.9599	30.9599	30.9432
	(2,3)	109.345	84.2732	47.8077	41.4794	41.4706	41.4706	41.4475
	(3,3)	144.375	106.561	57.1171	49.8046	49.7903	49.7903	49.7622
0.1	(1,1)	13.997	4.9582	2.1587	1.8542	1.8492	1.8492	1.8480
	(1,2)	22.545	8.1783	3.6851	3.2386	3.2217	3.2217	3.2196
	(1,3)	42.244	11.946	5.8204	5.2636	5.2270	5.2270	5.2234
	(2,2)	31.113	10.489	4.8601	4.3231	4.2925	4.2925	4.2894
	(2,3)	45.090	13.693	6.7667	6.1496	6.0989	6.0989	6.0942
	(3,3)	51.950	16.114	8.4305	7.7540	7.6834	7.6834	7.6762

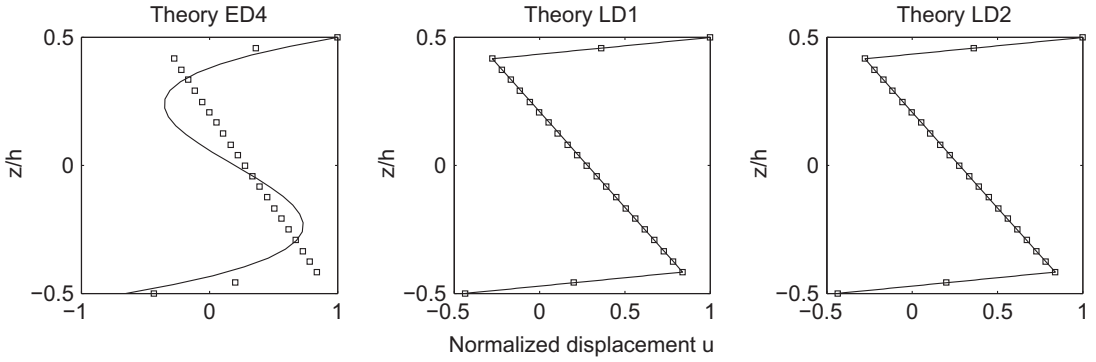

Fig. 4. Through-the-thickness distribution of normalized displacement $u(0,b/2)$ for the sandwich plate in Example 4 with $h/a = 0.1$ vibrating in the mode (1,1). Legend: – present analysis based on the plate theory specified in the figure title; □ reference values from [26].

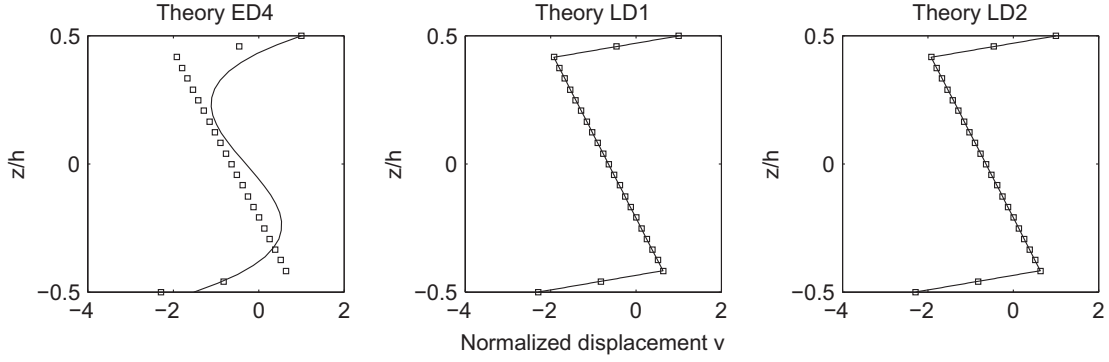

Fig. 5. Through-the-thickness distribution of normalized displacement $v(a/2,0)$ for the sandwich plate in Example 4 with $h/a = 0.1$ vibrating in the mode (1,1). Legend: – present analysis based on the plate theory specified in the figure title; □ reference values from [26].

quency parameters $\lambda = (\omega b^2/\pi^2 h)\sqrt{\rho/E_2}$ are shown in Table 6 for some LW theories of increasing order N and compared with solutions presented in [24], where a finite element model based on a higher-order shear deformation theory (HOST) is used, and with those available in [25], where a Ritz method based on FSDT is adopted.

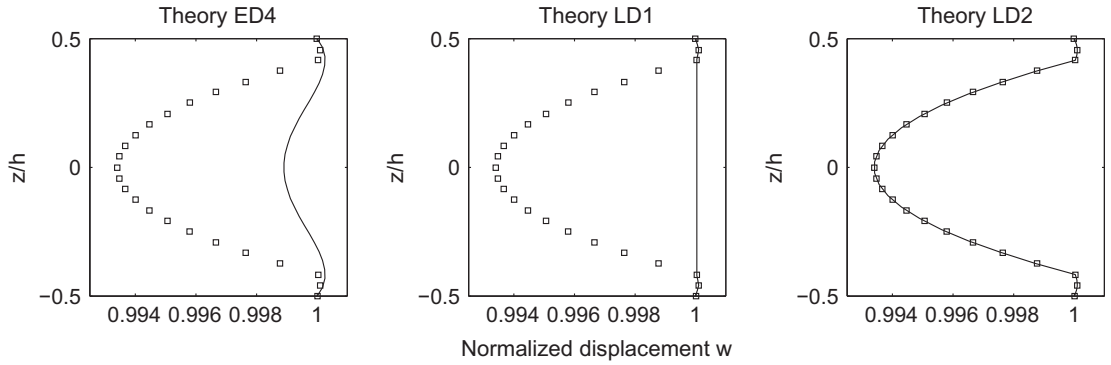

Fig. 6. Through-the-thickness distribution of normalized displacement $w(a/2,b/2)$ for the sandwich plate in Example 4 with $h/a = 0.1$ vibrating in the mode $(1,1)$. Legend: – present analysis based on the plate theory specified in the figure title; □ reference values from [26].

Table 9
First six frequency parameters $\lambda = \frac{\omega b^2}{h}\sqrt{\frac{\rho}{E_2}}$ of square moderately thick $(h/a = 0.1)$ sandwich plates with material properties in Table 7 and various boundary conditions.

Boundary conditions	Mode					
	1	2	3	4	5	6
SCSS	1.9481	3.2841	3.4885	4.5069	5.2699	5.6786
SCCS	2.0425	3.5459	3.5471	4.7124	5.7179	5.7190
SCCC	2.1619	3.6200	3.8500	4.9542	5.7678	6.2162
CCCC	2.2756	3.9180	3.9180	5.1853	6.2592	6.2647
CFFF	0.6786	1.2311	2.1670	2.5625	2.8120	3.6477
SFCS	1.5478	2.4914	3.2411	3.8863	4.0514	5.1892

Table 10
First six frequency parameters $\lambda = \frac{\omega b^2}{h}\sqrt{\frac{\rho}{E_2}}$ of fully clamped rhombic sandwich plates with material properties in Table 7 and various skew angles.

Skew angle (°)	Mode					
	1	2	3	4	5	6
5	2.2846	3.8750	3.9936	5.1918	6.2839	6.3111
10	2.3120	3.8632	4.1051	5.2138	6.3587	6.4516
15	2.3596	3.8831	4.2580	5.2579	6.4891	6.6886
30	2.6598	4.1696	5.0712	5.6130	7.2993	7.3328
45	3.3948	5.0292	6.6164	6.9412	8.3893	9.4581

It is to be noted that FSDT substantially overestimates natural frequencies for both cases and skew angles under investigation. As expected, this effect increases with increasing mode number. For example, the percentage error in the eighth frequency parameter between FSDT and LD3 models is above 6% in all cases. The use of refined models appears to be mandatory for higher mode evaluation of multilayered plates even though moderately thick plate geometries are considered. Although remarkable, the discrepancy becomes smaller if present layewise models are compared with those obtained by the equivalent single-layer HOST employed in [24]. Note also that, for skew plates, as the order of the theory increases accuracy gets improved significantly even for the fundamental frequency. This is probably due to the effect of corner stress singularities which occur as the skew angle becomes large.

5.4. Example 4: soft-core sandwich plates

A case involving the simply-supported rectangular sandwich plate analyzed in [26] is presented in this example. The plate has a [0°/90°/core/0°/90°] layup with material properties of the cross-ply faces and isotropic core listed in Table 7. It should be observed the large difference in stiffness between the core and the faces, which could undermine the classical assumption of the sandwich core to be incompressible in the vertical direction. In the case of a flexible or soft-core (for example, a foam core) sandwich plate, difficulties are known in capturing the correct dynamic behavior with simple kinematic models [27,28]. The ratio of thickness of the core to thickness of the face sheet is assumed to be 10 in this example. For the sake of comparison with results provided in [26], both cases of square thin $(h/a = 0.01)$ and moderately thick $(h/a = 0.1)$ plates are considered. Results are shown in Table 8 in terms of the non-dimensional frequency $\lambda = (\omega b^2/h)\sqrt{\rho/E_2}$ for some pairs of (m,n) wave numbers corresponding to the lowest vibration modes. Upper-bound solutions obtained by the present Ritz formulation with $P = 12$ are computed using many kinematic models, including the first-order shear deformation theory, the fourth and fifth-order ESL theories and three LW theories with $N = 1, 2, 3$.

Although errors are less for the lowest frequency parameters of the thin case compared to the thicker one, Table 8 clearly shows that results computed with FSDT and higher-order ESL theories grossly overestimate the natural frequencies in comparison with LW models both for thin and moderately thick plates. This is due to the large stiffness ratio between the skins and the core. The numerical investigation demonstrates that the discrepancy can be contrasted by the use of layerwise kinematics, which appears to be mandatory for sandwich plates with very soft core irrespective of the thickness-to-length ratio. It is also observed that a slight improvement in accuracy of natural frequencies is obtained by LD2 compared to LD1 theory, whereas no further improvement is detected by using a layerwise model of higher order.

As a further insight into these data, through-the-thickness variation of displacements corresponding to the first $(1,1)$ bending mode of vibration is presented for the case of $h/a = 0.1$. Fig. 4 shows distribution of in-plane displacement u at location $(0,b/2)$ as obtained by present method using three different kinematic models of increasing complexity and compared with reference values provided in [26]. Displacements in Fig. 4 have been normalized with respect to the component at the outer surface of the upper skin. Similarly, normalized in-plane displacement v at $(a/2,0)$ and normalized transverse displacement w at the center of the plate $(a/2,b/2)$ are depicted in Figs. 5 and 6, respectively. Graphical distribution clearly shows that sharp changes with discontinuous derivatives in the response quantities occurring in correspondence of the skin-to-core interface cannot be well approximated by ED4 model. The linear zig-zag variation of the in-plane displacements u and v is correctly captured by LD1 model. However, accurate prediction of the non-linear distribution of transverse displacement w in the face sheets and the sandwich core demands a layerwise

kinematic theory of second order. Although limited to a specific case, it is confirmed that refined models are especially required if one is also interested in confident evaluation of local through-the-thickness dynamic quantities, other that to global vibration parameters such as natural frequencies and mode shapes.

5.5. Example 5: new results for soft-core sandwich plates

The sandwich plate with laminated skins and soft isotropic core analyzed in the last example is here assumed to have different boundary conditions and in-plane geometry.

First, six cases involving square moderately thick ($h/a = 0.1$) plates with various combinations of classical boundary conditions are presented in Table 9. Non-dimensional frequency solutions $\lambda = (\omega b^2/h)\sqrt{\rho/E_2}$ are reported corresponding to the first six modes. According to what was previously observed, computations have been performed using a layerwise theory of order $N = 2$ with a Ritz expansion of degree $P = 12$. Therefore, results are considered to be highly accurate. A similar table based on a different kinematic model can be easily and quickly generated without any further mathematical development by adopting the formulation presented in this work. Note that frequency parameters of the modes in the range under investigation get higher, with respect to the simply-supported case, as the number of clamped edges increases. This is due to the higher constraints introduced at boundaries.

Finally, for the sake of future comparison, the first six natural frequencies of the soft-core sandwich plate with fully clamped boundary conditions are listed in Table 10 for some increasing values of the skew angle γ from 5° to 45°. The plate has aspect ratio $a/b = 1$ and thickness-to-length ratio $h/a = 0.1$. It is observed that all the reported vibration parameters increase as the skew angle becomes large.

6. Conclusions

The variable-kinematic Ritz-based approach introduced in [18] has been extended in this work to include layerwise theories and applied to the analysis of freely vibrating multilayered skew plates with arbitrary lamination layups and classical boundary conditions. The proposed technique relies on appropriate expansion of so-called Ritz fundamental nuclei of the mass and stiffness matrix, which are invariant with respect to the plate kinematic model and the type of Ritz trial functions. An entire family of higher-order layerwise and, as a special case, equivalent single-layer theories can be used to model the plate without the need of a different mathematical development for each different approach. Accurate upper-bound frequency solutions of laminated composite and sandwich plates have been presented using products of Chebyshev polynomials and basic boundary functions as admissible functions.

It has been shown that the method rate of convergence is rather high and it is not significantly affected by the assumed plate theory, i.e., well-converged frequency values have been obtained with roughly the same number of Ritz terms regardless of the order and type of kinematic model. It was observed that convergence of the method is faster for simply-supported plates, whereas plates involving clamped edges exhibit slower convergence rate.

From comparison results, it has been noted that Ritz-based models relying on equivalent single-layer theories of relatively low order yield reasonably accurate results of the first lowest frequency parameters for laminated composite plates. Layerwise models are instead strongly required for confident prediction of higher order modes of vibration, natural frequencies of thin and thick sandwich plates with soft core and accurate evaluation of through-the-thickness local distribution of displacements.

Appendix A

After introducing the following notation:

$$I^{ef}_{\alpha m\beta\bar{m}} = \int_{-1}^{+1} \frac{d^e}{d\xi^e}[\phi_{\alpha\tau m}(\xi)]\frac{d^f}{d\xi^f}[\phi_{\beta s\bar{m}}(\xi)]\,d\xi \quad m,\ \bar{m} = 1,2,\ldots,P \tag{40}$$

$$J^{ef}_{\alpha n\beta\bar{n}} = \int_{-1}^{+1} \frac{d^e}{d\eta^e}[\psi_{\alpha\tau n}(\eta)]\frac{d^f}{d\eta^f}[\psi_{\beta s\bar{n}}(\eta)]\,d\eta \quad n,\ \bar{n} = 1,2,\ldots,P \tag{41}$$

the nine terms of the Ritz stiffness nucleus can be explicitly written as

$$\begin{aligned}
K^k_{\tau sij}(1,1) &= \left(E^k_{\tau s}\widetilde{C}^k_{11}\frac{b}{a}\cos\gamma - 2E^k_{\tau s}\widetilde{C}^k_{16}\frac{b}{a}\sin\gamma + E^k_{\tau s}\widetilde{C}^k_{66}\frac{b}{a}\tan\gamma\sin\gamma\right)I^{11}_{umu\bar{m}}J^{00}_{un\bar{n}}\\
&+\left(E^k_{\tau s}\widetilde{C}^k_{16} - E^k_{\tau s}\widetilde{C}^k_{66}\tan\gamma\right)\left(I^{10}_{umu\bar{m}}J^{01}_{un\bar{n}} + I^{01}_{umu\bar{m}}J^{10}_{un\bar{n}}\right)\\
&+E^k_{\tau s}\widetilde{C}^k_{66}\frac{a}{b}\sec\gamma I^{00}_{umu\bar{m}}J^{11}_{un\bar{n}} + E^k_{\partial\tau\partial s}\widetilde{C}^k_{55}\frac{ab}{4}\cos\gamma I^{00}_{umu\bar{m}}J^{00}_{un\bar{n}}\\
K^k_{\tau sij}(1,2) &= \left(E^k_{\tau s}\widetilde{C}^k_{16}\frac{b}{a}\cos\gamma - E^k_{\tau s}\widetilde{C}^k_{12}\frac{b}{a}\sin\gamma - E^k_{\tau s}\widetilde{C}^k_{66}\frac{b}{a}\sin\gamma + E^k_{\tau s}\widetilde{C}^k_{26}\frac{b}{a}\tan\gamma\sin\gamma\right)I^{11}_{um\nu\bar{m}}J^{00}_{un\bar{n}}\\
&+\left(E^k_{\tau s}\widetilde{C}^k_{12} - E^k_{\tau s}\widetilde{C}^k_{26}\tan\gamma\right)I^{10}_{um\nu\bar{m}}J^{01}_{un\bar{n}} + \left(E^k_{\tau s}\widetilde{C}^k_{66} - E^k_{\tau s}\widetilde{C}^k_{26}\tan\gamma\right)I^{01}_{um\nu\bar{m}}J^{10}_{un\bar{n}}\\
&+E^k_{\tau s}\widetilde{C}^k_{26}\frac{a}{b}\sec\gamma I^{00}_{um\nu\bar{m}}J^{11}_{un\bar{n}} + E^k_{\partial\tau\partial s}\widetilde{C}^k_{45}\frac{ab}{4}\cos\gamma I^{00}_{um\nu\bar{m}}J^{00}_{un\bar{n}}\\
K^k_{\tau sij}(1,3) &= \left(E^k_{\tau\partial s}\widetilde{C}^k_{13}\frac{b}{2}\cos\gamma - E^k_{\tau\partial s}\widetilde{C}^k_{36}\frac{b}{2}\sin\gamma\right)I^{10}_{umw\bar{m}}J^{00}_{un\bar{n}} + E^k_{\tau\partial s}\widetilde{C}^k_{36}\frac{a}{2}I^{00}_{umw\bar{m}}J^{10}_{un\bar{n}}\\
&+\left(E^k_{\partial\tau s}\widetilde{C}^k_{55}\frac{b}{2}\cos\gamma - E^k_{\partial\tau s}\widetilde{C}^k_{45}\frac{b}{2}\sin\gamma\right)I^{01}_{umw\bar{m}}J^{00}_{un\bar{n}} + E^k_{\partial\tau s}\widetilde{C}^k_{45}\frac{a}{2}I^{00}_{umw\bar{m}}J^{01}_{un\bar{n}}\\
K^k_{\tau sij}(2,1) &= \left(E^k_{\tau s}\widetilde{C}^k_{16}\frac{b}{a}\cos\gamma - E^k_{\tau s}\widetilde{C}^k_{12}\frac{b}{a}\sin\gamma - E^k_{\tau s}\widetilde{C}^k_{66}\frac{b}{a}\sin\gamma + E^k_{\tau s}\widetilde{C}^k_{26}\frac{b}{a}\tan\gamma\sin\gamma\right)I^{11}_{vmu\bar{m}}J^{00}_{vnu\bar{n}}\\
&+\left(E^k_{\tau s}\widetilde{C}^k_{12} - E^k_{\tau s}\widetilde{C}^k_{26}\tan\gamma\right)I^{01}_{vmu\bar{m}}J^{10}_{vnu\bar{n}} + \left(E^k_{\tau s}\widetilde{C}^k_{66} - E^k_{\tau s}\widetilde{C}^k_{26}\tan\gamma\right)I^{10}_{vmu\bar{m}}J^{01}_{vnu\bar{n}}\\
&+E^k_{\tau s}\widetilde{C}^k_{26}\frac{a}{b}\sec\gamma I^{00}_{vmu\bar{m}}J^{11}_{vnu\bar{n}} + E^k_{\partial\tau\partial s}\widetilde{C}^k_{45}\frac{ab}{4}\cos\gamma I^{00}_{vmu\bar{m}}J^{00}_{vnu\bar{n}}\\
K^k_{\tau sij}(2,2) &= \left(E^k_{\tau s}\widetilde{C}^k_{66}\frac{b}{a}\cos\gamma - 2E^k_{\tau s}\widetilde{C}^k_{26}\frac{b}{a}\sin\gamma + E^k_{\tau s}\widetilde{C}^k_{22}\frac{b}{a}\tan\gamma\sin\gamma\right)I^{11}_{vm\nu\bar{m}}J^{00}_{vn\bar{n}}\\
&+\left(E^k_{\tau s}\widetilde{C}^k_{26} - E^k_{\tau s}\widetilde{C}^k_{22}\tan\gamma\right)\left(I^{10}_{vm\nu\bar{m}}J^{01}_{vn\bar{n}} + I^{01}_{vm\nu\bar{m}}J^{10}_{vn\bar{n}}\right)\\
&+E^k_{\tau s}\widetilde{C}^k_{22}\frac{a}{b}\sec\gamma I^{00}_{vm\nu\bar{m}}J^{11}_{vn\bar{n}} + E^k_{\partial\tau\partial s}\widetilde{C}^k_{44}\frac{ab}{4}\cos\gamma I^{00}_{vm\nu\bar{m}}J^{00}_{vn\bar{n}}\\
K^k_{\tau sij}(2,3) &= \left(E^k_{\tau\partial s}\widetilde{C}^k_{36}\frac{b}{2}\cos\gamma - E^k_{\tau\partial s}\widetilde{C}^k_{23}\frac{b}{2}\sin\gamma\right)I^{10}_{vmw\bar{m}}J^{00}_{vn\bar{n}} + E^k_{\tau\partial s}\widetilde{C}^k_{23}\frac{a}{2}I^{00}_{vmw\bar{m}}J^{10}_{vn\bar{n}}\\
&+\left(E^k_{\partial\tau s}\widetilde{C}^k_{45}\frac{b}{2}\cos\gamma - E^k_{\partial\tau s}\widetilde{C}^k_{44}\frac{b}{2}\sin\gamma\right)I^{01}_{vmw\bar{m}}J^{00}_{vn\bar{n}} + E^k_{\partial\tau s}\widetilde{C}^k_{44}\frac{a}{2}I^{00}_{vmw\bar{m}}J^{01}_{vn\bar{n}}\\
K^k_{\tau sij}(3,1) &= \left(E^k_{\tau\partial s}\widetilde{C}^k_{55}\frac{b}{2}\cos\gamma - E^k_{\tau\partial s}\widetilde{C}^k_{45}\frac{b}{2}\sin\gamma\right)I^{10}_{wmu\bar{m}}J^{00}_{wnu\bar{n}} + E^k_{\tau\partial s}\widetilde{C}^k_{45}\frac{a}{2}I^{00}_{wmu\bar{m}}J^{10}_{wnu\bar{n}}\\
&+\left(E^k_{\partial\tau s}\widetilde{C}^k_{13}\frac{b}{2}\cos\gamma - E^k_{\partial\tau s}\widetilde{C}^k_{36}\frac{b}{2}\sin\gamma\right)I^{01}_{wmu\bar{m}}J^{00}_{wnu\bar{n}} + E^k_{\partial\tau s}\widetilde{C}^k_{36}\frac{a}{2}I^{00}_{wmu\bar{m}}J^{01}_{wnu\bar{n}}\\
K^k_{\tau sij}(3,2) &= \left(E^k_{\tau\partial s}\widetilde{C}^k_{45}\frac{b}{2}\cos\gamma - E^k_{\tau\partial s}\widetilde{C}^k_{44}\frac{b}{2}\sin\gamma\right)I^{10}_{wm\nu\bar{m}}J^{00}_{wn\bar{n}} + E^k_{\tau\partial s}\widetilde{C}^k_{44}\frac{a}{2}I^{00}_{wm\nu\bar{m}}J^{10}_{wn\bar{n}}\\
&+\left(E^k_{\partial\tau s}\widetilde{C}^k_{36}\frac{b}{2}\cos\gamma - E^k_{\partial\tau s}\widetilde{C}^k_{23}\frac{b}{2}\sin\gamma\right)I^{01}_{wm\nu\bar{m}}J^{00}_{wn\bar{n}} + E^k_{\partial\tau s}\widetilde{C}^k_{23}\frac{a}{2}I^{00}_{wm\nu\bar{m}}J^{01}_{wn\bar{n}}\\
K^k_{\tau sij}(3,3) &= \left(E^k_{\tau s}\widetilde{C}^k_{55}\frac{b}{a}\cos\gamma - 2E^k_{\tau s}\widetilde{C}^k_{45}\frac{b}{a}\sin\gamma + E^k_{\tau s}\widetilde{C}^k_{44}\frac{b}{a}\tan\gamma\sin\gamma\right)I^{11}_{wmw\bar{m}}J^{00}_{wn\bar{n}}\\
&+\left(E^k_{\tau s}\widetilde{C}^k_{45} - E^k_{\tau s}\widetilde{C}^k_{44}\tan\gamma\right)\left(I^{10}_{wmw\bar{m}}J^{01}_{wn\bar{n}} + I^{01}_{wmw\bar{m}}J^{10}_{wn\bar{n}}\right)\\
&+E^k_{\tau s}\widetilde{C}^k_{44}\frac{a}{b}\sec\gamma I^{00}_{wmw\bar{m}}J^{11}_{wn\bar{n}} + E^k_{\partial\tau\partial s}\widetilde{C}^k_{33}\frac{ab}{4}\cos\gamma I^{00}_{wmw\bar{m}}J^{00}_{wn\bar{n}}
\end{aligned}$$

The explicit expression of the non-null terms of the mass Ritz nucleus are given below:

$$M^k_{\tau sij}(1,1) = E^k_{\tau s}\rho^k\frac{ab}{4}\cos\gamma I^{00}_{umu\bar{m}}J^{00}_{un\bar{n}}$$

$$M^k_{\tau sij}(2,2) = E^k_{\tau s}\rho^k\frac{ab}{4}\cos\gamma I^{00}_{vm\nu\bar{m}}J^{00}_{vn\bar{n}}$$

$$M^k_{\tau sij}(3,3) = E^k_{\tau s}\rho^k\frac{ab}{4}\cos\gamma I^{00}_{wmw\bar{m}}J^{00}_{wn\bar{n}}$$

Integrals in Eqs. (40) and (41) have been numerically evaluated through standard Gauss quadrature.

References

[1] Kirchhoff G. Über das Gleichgewicht und die Bewegung einer elastischen Scheibe. Journal für die reine und angewandte Mathematik 1850;40:51–88.

[2] Mindlin RD. Influence of rotary inertia and shear on flexural motions of isotropic, elastic plates. J Appl Mech 1951;18:1031–6.
[3] Yang P, Norris CH, Stavsky Y. Elastic propagation in heterogeneous plates. Int J Solids Struct 1966;2:665–84.
[4] Carrera E. Theories and finite elements for multilayered, anisotropic, composite plates and shells. Arch Comput Methods Eng 2002;9:87–140.
[5] Noor AK, Burton WS. Assessment of shear deformation theories for multilayered composite plates. Appl Mech Rev 1989;41:1–18.
[6] Reddy JN, Robbins DH. Theories and computational models for composite laminates. Appl Mech Rev 1994;47:147–65.
[7] Carrera E. Historical review of zig-zag theories for multilayered plates and shells. Appl Mech Rev 2003;56:287–308.
[8] Reddy JN, Arciniega RA. Shear deformation plate and shell theories: from Stavsky to present. Mech Adv Mater Struct 2004;11:535–82.
[9] Wanji C, Zhen W. A selective review on recent development of displacement-based laminated plate theories. Recent Patents Mech Eng 2008;1:29–44.
[10] Zhang YX, Yang CH. Recent developments in finite element analysis for laminated composite plates. Compos Struct 2009;88:147–57.
[11] Carrera E. A class of two dimensional theories for multilayered plates analysis. Atti Accademia delle Scienze di Torino. Memorie Scienze Fisiche 1995;1920:49–87.
[12] Carrera E. An assessment of mixed and classical theories on global and local response of multilayered orthotropic plates. Compos Struct 2000;50:183–98.
[13] Carrera E, Ciuffreda A. A unified formulation to assess theories of multilayered plates for various bending problems. Compos Struct 2005;69:271–93.
[14] Nali P, Carrera E, Lecca S. Assessments of refined theories for buckling analysis of laminated plates. Compos Struct 2011;93:456–64.
[15] Carrera E, Miglioretti F, Petrolo M. Accuracy of refined finite elements for laminated plate analysis. Compos Struct 2011;93:1311–27.
[16] Ferreira AJM, C Roque CM, Carrera E, Cinefra M. Analysis of thick isotropic and cross-ply laminated plates by radial basis functions and a unified formulation. J Sound Vib 2011;330:771–87.
[17] Ferreira AJM, C Roque CM, Carrera E, Cinefra M, Polit O. Analysis of laminated plates by trigonometric theory, radial basis, and unified formulation. AIAA J 2011;49:1559–62.
[18] Dozio L, Carrera E. A variable kinematic Ritz formulation for vibration study of quadrilateral plates with arbitrary thickness. J Sound Vib 2011;330:4611–32.
[19] Fazzolari FA, Carrera E. Advanced variable kinematics Ritz and Galerkin formulations for accurate buckling and vibration analysis of anisotropic laminated composite plates. Compos Struct 2011;94:50–67.
[20] Reddy JN. Mechanics of laminated composite plates and shells. CRC Press; 2004.
[21] Zhou D, Cheung YK, Au FTK, Lo SH. Three-dimensional vibration analysis of thick rectangular plates using Chebyshev polynomial and Ritz method. Int J Solids Struct 2002;39:6339–53.
[22] Chen WQ, Lue CF. 3D free vibration analysis of cross-ply laminated plates with one pair of opposite edges simply supported. Compos Struct 2005;69:77–87.
[23] Demasi L. Quasi-3D analysis of free vibration of anisotropic plates. Compos Struct 2006;74:449–57.
[24] Garg AK, Khare RK, Kant T. Free vibration of skew fiber-reinforced composite and sandwich laminates using a shear deformable finite element method. J Sandwich Struct Mater 2006;8:33–52.
[25] Wang S. Free vibration analysis of skew fibre-reinforced composite laminates based on first-order shear deformation plate theory. Comput Struct 1997;63:525–38.
[26] Rao MK, Desai YM. Analytical solutions for vibrations of laminated and sandwich plates using mixed theory. Compos Struct 2004;63:361–73.
[27] Frostig Y, Thomsen OT. Higher-order free vibration of sandwich panels with a flexible core. Int J Solids Struct 2004;41:1697–724.
[28] Carrera E, Brischetto S. A survey with numerical assessment of classical and refined theories for the analysis of sandwich plates. Appl Mech Rev 2009;62:010803-1–010803-17.